Journal of Hydroscience and Hydraulic Engineering
Vol. 30, No.1 May, 2012, 77-86

NUMERICAL STUDY ON SEAWATER INTRUSION IN NON-UNIFORM AQUIFER

By

Masahiko Saito

Kobe University, Rokkodai-cho Nada, Kobe, Japan

Yusuke Takayama

Kobe University, Rokkodai-cho Nada, Kobe, Japan

and

Kei Nakagawa

Nagasaki University, Bunkyomachi, Nagasaki, Japan

SYNOPSIS

Knowledge of seawater intrusion to aquifers is very important for the efficient use of groundwater in coastal areas. Conventional numerical simulations of seawater intrusion were performed mostly in uniform porous media. However, it is known that hydraulic conductivity varies spatially. The objective of this paper is to investigate seawater intrusion behavior in non-uniform porous media by means of numerical simulations using the spatial distribution model for hydraulic conductivity. Findings show that the length of seawater intrusion is affected by the shape of permeability distribution. When the aquifer has a laminar structure of permeability, the change of seawater intrusion length is smaller than the general aquifer.

INTRODUCTION

Groundwater salination has been reported in the coastal areas of many countries.[1)-5)] The Intergovernmental Panel on Climate Change(IPCC) has estimated that global sea level may rise by 0.09 to 0.88m by 2100.[6), 7)] Coastal groundwater in particular is directly affected by the rise in sea levels accompanying global warming, and finding a means of rapid assessment of coastal groundwater quality is a paramount importance for the proposal of measures for its preservation.

Although various approaches have been used to investigate coastal groundwater salination phenomenon, such as, numerical simulations[8), 9)], laboratory-scale experiments[10)], or onsite measurements[11)], little consideration has been given to ground non-uniformity. Clearly stratified ground has been treated as a multilayer structure, but with uniformity assumed for each layer[12)-13)]. However, the actual ground is inherently non-uniform, and the results of analyses assuming its uniformity

must therefore be regarded as averages. Analyses may not correctly reproduce or predict the actual phenomena, and no clear findings on the effects of ground non-uniformity on seawater intrusion have been obtained.

In the present study, we investigate seawater intrusion in non-uniform unconfined aquifers. Using a model of permeability spatial distribution, we first generate a numerically inhomogeneous field and investigate the influence of differing permeability distribution patterns and the size of their differences on seawater intrusion. Next, we consider cases in which the mean hydraulic gradient of coastal groundwater changes due to variations in sea levels and then we investigate the effect of this change in gradient and ground non-uniformity on the size of the seawater intrusion area. In addition, we consider cases of anisotropic permeability distribution.

GOVERNING EQUATION

Saturated-unsaturated seepage analysis

The governing equation of saturated-unsaturated seepage with consideration given to density variation may be written as follows[14)-16)]:

$$\frac{\rho}{\rho_0}\left(\beta S_s+\phi\frac{dS_w}{d\psi}\right)\frac{\partial\psi}{\partial t}=\nabla\cdot\left\{\mathbf{K}\cdot\left(\nabla\psi+\frac{\rho}{\rho_0}\nabla Z\right)\right\} \tag{1}$$

where ρ denotes the aqueous solution density at concentration C, ρ_0 is the density of water at concentration 0, ψ is the pressure head, Z is the elevation head, **K** is the hydraulic conductivity tensor, ϕ is the porosity, S_s is the specific storage, and t is the time. In the saturated region (S_w=1), β=1; in the unsaturated region ($S_w \neq 1$), β=0. The hydraulic conductivity tensor may be expressed as follows in terms of the relative permeability k_r and the saturated hydraulic conductivity tensor **Ks**.

$$\mathbf{K} = k_r \cdot \mathbf{Ks} \tag{2}$$

The boundary conditions were

$$\psi = \psi_1 \text{ on } \Gamma_1 \tag{3}$$

on the prescribed-pressure boundary Γ_1 and

$$q = q_2 = -\mathbf{n}\cdot\mathbf{K}\cdot(\nabla\psi+\nabla Z) \text{ on } \Gamma_2 \tag{4}$$

on the prescribed-flux (q) boundary Γ_2 where **n** is the outwardly directed unit normal vector on the boundary.

Soil Water Retention Curve

The equation of van Genuchten[17)] was used to express the water retention curve necessary for the analysis, as

$$S_e = \frac{S_w - S_r}{1 - S_r} = \left\{1 + (\alpha\psi_c)^n\right\}^{-m} \tag{5}$$

where ψ_c ($= -\psi$) denotes the capillary pressure, S_e is the effective saturation, S_r is the residual saturation, and α, n, m are the geometry parameters with n, m is dimensionless, α has the dimension of inverse pressure head, and n and m is in the relationship $m = 1 - 1/n$.

The relative permeability and the effective saturation are related as follows[18]:

$$k_r = S_e^{\varepsilon}\left\{1 - \left(1 - S_e^{1/m}\right)^m\right\}^2 \tag{6}$$

where parameter ε represents pore continuity and is expressed as ε=1/2. By differentiating Eq. (5) with respect to ψ_c and rearranging, we obtain the following:

$$-\phi\frac{dS_w}{d\psi_c} = \phi\alpha mn(1 - S_r)(\alpha\psi_c)^{n-1}\left\{1 + (\alpha\psi_c)^n\right\}^{-m-1} \tag{7}$$

Advection dispersion equation

The movement of soluble materials by groundwater flow can be expressed by the following governing equation (the advection-dispersion equation).

$$\theta\frac{\partial C}{\partial t} = \nabla\cdot(\theta\mathbf{D}\cdot\nabla C) - \mathbf{q}\cdot\nabla C \tag{8}$$

where C denotes the concentration, θ is the volumetric water content ($=\phi S_w$), $\mathbf{D}$ is the dispersion coefficient tensor, and $\mathbf{q}$ is the Darcy velocity vector. Component D_{ij} of $\mathbf{D}$ in Eq. (8) may be given as[19]

$$\theta D_{ij} = \alpha_T|\mathbf{q}|\delta_{ij} + (\alpha_L - \alpha_T)\frac{q_i\cdot q_j}{|\mathbf{q}|} + D_m\theta\delta_{ij} \tag{9}$$

where α_L is the longitudinal dispersivity, α_T is the transverse dispersivity, q_i is the component of Darcy velocity vector $\mathbf{q}$ in direction i, D_m is the molecular diffusion coefficient, and δ_{ij} is the component of the Kronecker delta tensor.

The boundary conditions were

$$C = C_A \text{ on } \Gamma_A \tag{10}$$

on the prescribed-concentration boundary,

$$F = F_B = -\mathbf{n}\cdot(\theta\mathbf{D}\cdot\nabla C) \quad \text{on} \quad \Gamma_B \tag{11}$$

on the prescribed concentration-gradient boundary, and

$$F = F_C = \mathbf{n}\cdot(\mathbf{q}C - \theta\mathbf{D}\cdot\nabla C) \quad \text{on } \Gamma_C \tag{12}$$

on the prescribed flow-velocity boundary.

Density ρ of Eq. (1) can be obtained as a function of concentration C, as

$$\rho = \rho_0 + (\rho_s - \rho_0)\frac{C}{C_s} \tag{13}$$

where ρ_s denotes the seawater density and C_s is its concentration.

It is known that if Eq. (9) is discretized by the standard Galerkin method, the solution is unstable when the advection term is dominant. Therefore, in the present study, we used the explicit characteristic Galerkin method.[20)]

Spatial distribution model of hydraulic conductivity

We generated a model of spatial distribution of permeability using a spatial distribution model based on the stochastic fractal model proposed by Saito et al.[21)-23)] In this model, the equation of the power spectral density function of the logarithmic transformation value (Y=log(k_s)) of hydraulic conductivity takes the following form with $f^{-\zeta}$, and it has been shown that the spatial distribution of permeability in the ground can be easily simulated on this basis.

$$S(|\boldsymbol{f}|) \propto |\boldsymbol{f}|^{-\zeta} \tag{14}$$

where $\boldsymbol{f}$ is the wave number vector, $S(|\boldsymbol{f}|)$ is the power spectral density, and ζ is a parameter representing the spatial correlation and in a 2-dimensional model $\zeta \approx 2$. At this time, the correlation length (integral characteristic distance) in the case of approximation of the autocorrelation function by the exponential function is approximately 0.1 times the scale of the analysis domain. If we take the f_x and f_z components of $\boldsymbol{f}$ from Eq. (14) as

$$|\boldsymbol{f}| = \sqrt{f_x^2 + f_z^2} \tag{15}$$

then to introduce anisotropy between the x- and z-directions we add the parameter ω ($0<\omega\leq 1$) and modify Eq. (15) as

$$|\boldsymbol{f}| = \sqrt{f_x^2 + (\omega f_z)^2} \tag{16}$$

ANALYTICAL CONDITIONS

Analysis domain and boundary conditions

The analysis domain and boundary conditions are shown schematically in Fig. 1. The analysis domain is taken as a 2-

dimensional unconfined aquifer with a cross-section of 100 m length and 40 m height, an upstream (freshwater) water level of 37.2 m, and a downstream (seawater) level H_s. The mesh is composed of 4,000 elements, each 1 m × 1 m square. As boundary conditions for seepage analysis, we assume an impermeable boundary at z=0 m and a hydrostatic pressure distribution with consideration for the difference in density between seawater and freshwater both upstream and downstream. The downstream seepage face is taken as $z>H_s$, the freshwater density as ρ_0=1000 kg/m^3, and the seawater S.G. as 1.025. For the advection dispersion analysis, we take $\mathbf{n}\cdot(\mathbf{q}C-\theta\mathbf{D}\cdot\nabla C)=0$ at $z=0$ and the prescribed-concentration boundary ($C=0$) upstream and $C=C_s=1$ in the region of seawater inflow ($q\geq 0$) and $-\mathbf{n}\cdot(\theta\mathbf{D}\cdot\nabla C)=0$ in the region of outflow ($q<0$) downstream.

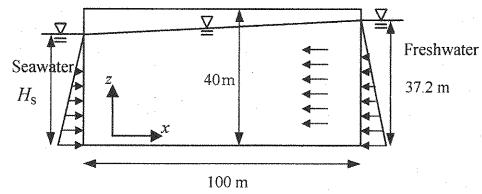

Fig. 1. Analysis domain and boundary conditions schematic.

Physical properties of ground

The hydraulic conductivity distribution is generated by using the permeability spatial distribution model. Here, the hydraulic conductivity allotted to each element is taken as isotropic with a geometric mean of K_{sa}=1.0×10^{-4} m/s.

The dispersivities of Eq. (9), with consideration limited to microscopic dispersion, are expressed as α_L = 6.0×10^{-2} m and α_T= 6.0×10^{-3} m, and the molecular diffusion coefficient is given as D_m= 1.0×10^{-9} m^2/s.

Analytical cases

An analysis was performed for three basic cases: the homogeneous field as Run-0, the isotropic inhomogeneous field as Run-1, and the anisotropic inhomogeneous field as Run-2. For the anisotropic inhomogeneous field, we assumed that the permeability in the horizontal direction would exhibit a layered distribution. For both Run-1 and Run-2, we generated 10 different types of spatial distributions using different random number sequences, and we investigated the spatial distribution for a total of 20 types of distribution using log(K_s/K_{sa}) positive/negative sign inversions.

ANALYTICAL RESULTS AND DISCUSSION

Isotropic inhomogeneous field

Fig. 2 shows the saltwater concentration distribution in Run-0 at 360 days after the beginning of the calculation considered it as a steady state with the seawater level H_s= 36 m. At z = 0, with L_s defined as the x coordinate of the point at which the seawater intrusion length reached its maximum at C=0.5 and L_{s0} defined as the maximum seawater intrusion length in Run-0, we found L_{s0}=45.8 m.

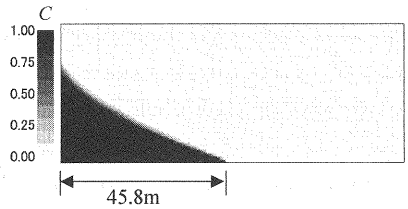

Fig. 2. Saltwater concentration distribution in homogeneous field, H_s=36 m.

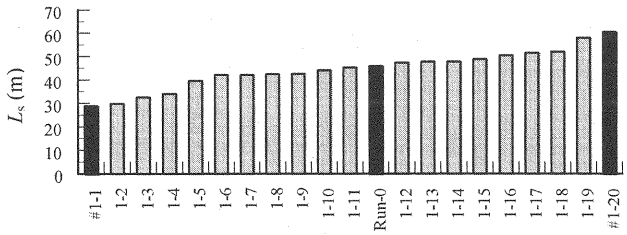

Fig. 3. Maximum seawater intrusion length L_s, Run-1.

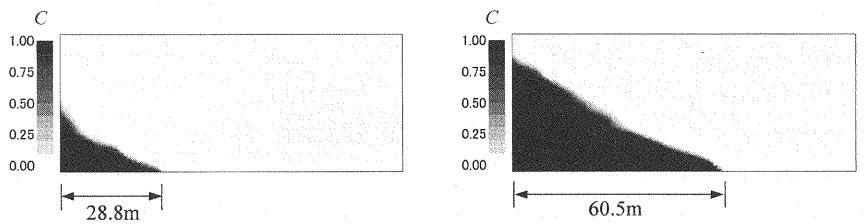

(a) #1-1 (b) #1-20

Fig. 4. Saltwater concentration distributions in inhomogeneous field. (H_s=36 m)

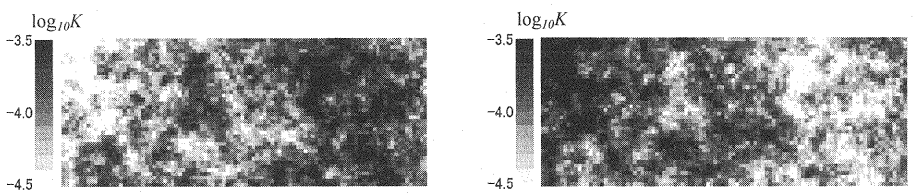

(a) #1-1 (b) #1-20

Fig. 5. Hydraulic conductivity distributions, #1-1 and #1-20.

Fig. 3 shows the values obtained for L_s, in order of decreasing size, in Run-1 #1-1~#1-20 in the case of $\log_{10}K_s$ variance σ^2=0.09 and H_s=36 m, for 20 types of inhomogeneous fields. The mean value of L_s was 44.3 m and the standard deviation was 8.6 m.

Fig. 4 shows the concentration distributions of #1-1 and #1-20, which exhibited the minimum (28.8 m) and maximum (60.5 m) values of L_s, respectively. As shown by their hydraulic conductivity distributions in Fig. 5, $\log K_s/K_{sa}$ positive/negative sign inversion is exhibited for the same spatial distribution. Such distributions are distinguished by the clear upstream and downstream separation of high-permeability and low-permeability regions. Fig. 6 shows the permeability distribution found for #1-11, in which L_s was approximately the same as in the homogeneous field. A

comparison shows that the size of the seawater intrusion region can differ greatly between two grounds which have the same stochastic properties, depending on their distribution profiles.

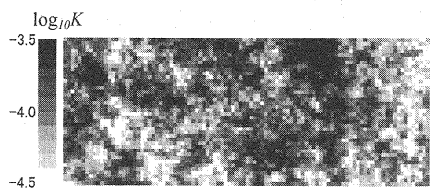

Fig. 6. Hydraulic conductivity distribution, #1-11.

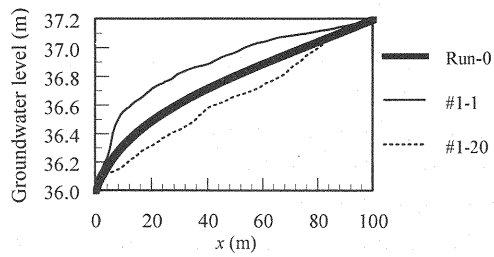

Fig. 7. Comparison of groundwater level distributions.

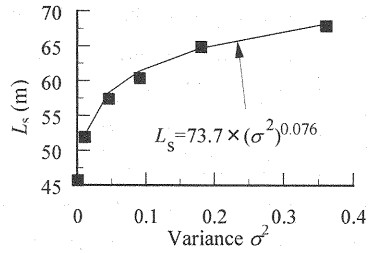

Fig. 8. Variance and seawater intrusion length.

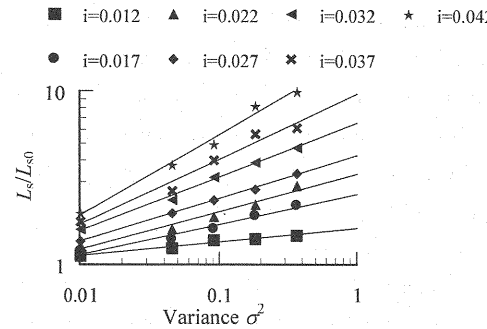

Fig. 9. Variance, mean hydraulic gradient, and L_s/L_{s0} (Run-1).

Fig. 7 is a comparison of the groundwater level distributions in Run-0, #1-1, and #1-20. In #1-1, as the permeability near the downstream end is low, the hydraulic gradient in that neighborhood is large and the groundwater level is generally higher than in Run-0. In #1-20, however, the hydraulic gradient is large upstream, and the groundwater level is generally lower than in Run-0. In both cases, the difference in water levels from Run-0 is at most approximately 0.2 m, but the difference between the two in seawater intrusion length is 10 m or more. In view of this, the following Ghyben-Herzberg equation may be of reference.[24)]

$$h_s = \frac{\rho_f}{\rho_s - \rho_f} h_f \tag{17}$$

where h_s is the depth relative to sea level at which the freshwater-saltwater boundary was found, h_f is the freshwater level relative to sea level, and ρ_f and ρ_s are respectively the freshwater and seawater densities. With ρ_f=1000 kg/m^3 and ρ_s=1025 kg/m^3, the freshwater-saltwater boundary depth h_s is then 40 times the freshwater level h_f.

This calculation thus also indicates that the seawater intrusion length may change substantially when a small change occurs at the freshwater level.

Fig. 8 shows the change in L_s when the permeability as represented by the $\log_{10}K_s$ variance σ^2 was varied between 0.01 and 0.36 for #1-20, thus indicating L_s dependence as a power function of σ^2. Fig. 9 is a systematic representation of the relation between changes in the seawater level H_s between 33.5 m and 36 m and the mean hydraulic gradient i (i = (37.2

- H_s)/100), the variance σ^2, and the ratio of L_s to L_{s0}. It indicates that when i has decreased (i.e., the seawater level has increased), although the influence of non-homogeneity tends to lessen, a difference of approximately 10%~50% occurs in the seawater intrusion length in a homogeneous field even with a mean hydraulic gradient of approximately 1/100.

Anisotropic inhomogeneous fields

Next, we applied anisotropy by assigning a value of 0.1 to ω in Eq. (16) and investigated cases of layered permeability layered distribution. Fig. 10 shows in decreasing order the values of L_s, in #2-1~#2-20 obtained in Run-2 for to the 20 types of inhomogeneous fields, assuming $\log_{10}K_s$ variance σ^2=0.09 and H_s=36 m. The mean value of L_s was 43.5 m, with a standard deviation of 5.2 m. As compared with the isotropic inhomogeneous field, the mean value was nearly the same but the standard deviation was smaller and the overall the influence of non-homogeneity thus lessened.

Fig. 11 shows the saltwater concentration distribution found for #2-20, in which L_s was largest, and Fig. 12 shows its permeability distribution. A moderate and partial bias toward higher permeability upstream can be seen, but as also shown for #1-20 in Fig. 5(b), no predominant bias is observable. This suggests that the reason for this is that the difference from the homogeneous field is small. As shown by the comparison of groundwater level distributions in Fig. 13, the groundwater level in #2-20 as compared with that of the homogeneous field (Run-0) was nearly identical near the downstream end (x < 10 m) and approximately 0.1 m lower in the range x=20~80 m.

Fig. 14, like Fig. 9, is a systematic representation of the relation found between the mean hydraulic gradient i, the variance σ^2, and the ratio of L_s to L_{s0} when the seawater level H_s was varied between 33.5 m and 36 m. Here, the influence of non-homogeneity also tends to lessen as the value of i decreases, and at approximately i=1/100 the seawater intrusion distance is only approximately 10% above that of the homogeneous field. This suggests that, within the range of conditions investigated in the present study, the treatment of layered distributions as homogeneous fields would generally not tend to give rise to substantial problems.

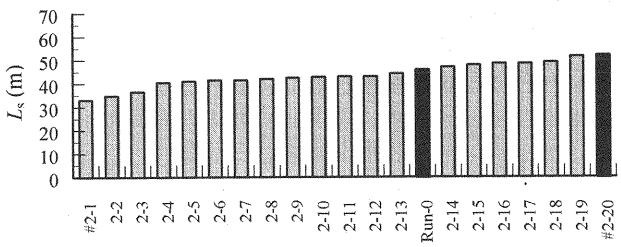

Fig. 10. Maximum seawater intrusion length L_s (Run-2).

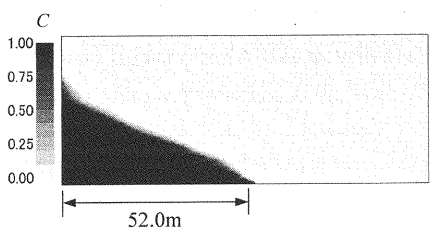

Fig. 11. Saltwater concentration distribution in inhomogeneous field, #2-20.

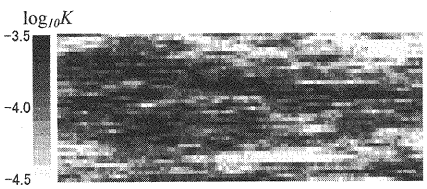

Fig. 12. Hydraulic conductivity distribution, #2-20.

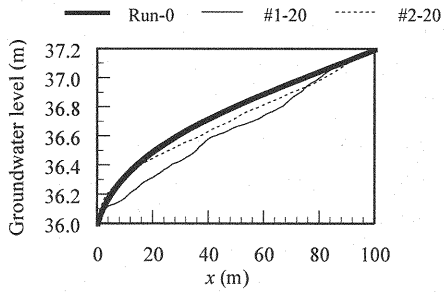

Fig. 13. Groundwater level distributions in Run-0, #1-20, and #2-20.

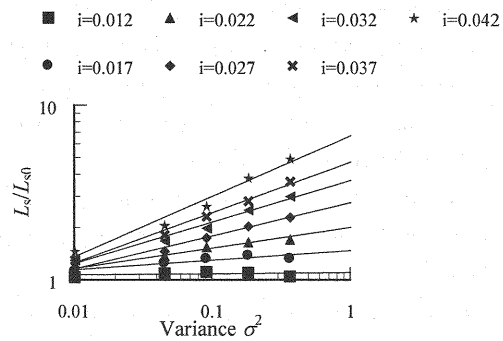

Fig. 14. Variance, mean hydraulic gradient, and L_s/L_{s0}, in Run-2.

CONCLUSIONS

In the present study, we considered the problem of seawater intrusion in non-uniform unconfined aquifers and investigated the influence of different patterns of permeability spatial distribution as well as the size of these differences on seawater intrusion. We also examined the influence of changes at sea levels by investigating the relation between the mean hydraulic gradient of coastal groundwater and ground non-uniformity, and investigated the case of anisotropy in permeability spatial distribution. We can draw the following conclusions from our investigations:

1) The seawater intrusion regions in different grounds may differ greatly even if they are of a stochastically identical nature, depending on their distribution patterns.
2) The seawater intrusion length may differ by 10 m or more between different grounds even if their groundwater levels differ by as little as 0.2 m.
3) Although the influence of ground non-uniformity tends to lessen if the mean hydraulic gradient in areas near the coast decreases (i.e., if the seawater level rises), non-uniformity may lead to an increase of 10%~50% in seawater intrusion length over that in uniform ground at a mean hydraulic gradient as small as 1/100.
4) In the case of layered permeability distribution, non-uniformity tends to exhibit no discernible influence under comparison with isotropic distribution.

REFERENCES

1. Water Resources Department National Land Agency: Nippon no Mizushigen, Government Printing Bureau, p.201, 1996. (in Japanese)
2. Xue, Y., Xie, C. and Wu, J. : A three-dimensional miscible transport model for seawater intrusion in China, Water Resour. Res., Vol.31, NO.4, pp.903-912, 1995.
3. Yakirevich, A., Melloul, A., Sorek, S., Shaath, S. and Borisov, V.: Simulation of seawater intrusion into the Khan Yunis area of the Gaza Strip coastal aquifer, Hydrogeology Journal, 6, pp.549–559, 1998.
4. Jin-Yong Lee and Sung-Ho Song: Groundwater chemistry and ionic ratios in a western coastal aquifer of Buan, Korea: implication for seawater intrusion, Geosciences Journal, Vol.11, No.3, pp. 259- 270, 2007.

5. Narayan, K. A., Schleeberger, C. and Bristow, K. L.: Modelling seawater intrusion in the Burdekin Delta Irrigation Area, North Queensland, Australia, Agricultural Water Management, 89, pp.217-228, 2007.
6. Intergovernmental Panel on Climate Change(IPCC): Climate Change 2001: The scientific basis. Contribution of Working Group I to the Third Assessment Report of the IPCC, 2001.
7. Intergovernmental Panel on Climate Change(IPCC): The regional impacts of climate change: An assessment of vulnerability. Contribution of Working Group II to the Second Assessment Report of the IPCC, 2001.
8. Kawatani,T.: Numerical Analysis of The Ground Water Mound and Fresh-Salt Water Interface in A Coastal Aquifer, Proc. of JSCE, No.238, pp.89-98, 1975.
9. Voss, C. I. and Souza, W. R.: Variable density flow and solute transport simulation of regional aquifers containing a narrow freshwater-saltwater transition zone, Water Resour. Res., Vol.23, No.10, pp.1851-1866, 1987.
10. Luyun Jr., R., Momii, K. and Nakagawa, K.: Laboratory-scale saltwater behavior due to subsurface cutoff wall, Journal of Hydrology, 377, pp.227-236, 2009.
11. Abarca, E., E. Va´zquez-Sun˜e´, J. Carrera, B. Capino, D. Ga´mez, and F. Batlle: Optimal design of measures to correct seawater intrusion, Water Resour. Res., 42, W09415, doi:10.1029/2005WR004524., 2006.
12. Collins, M. A. and Gelhar, L. W.: Seawater Intrusion in layered aquifers, Water Resour. Res., Vol.7, No.4, pp.971-979, 1971.
13. Kawatani,T. and Saito, M.: FEM analysis of seawater intrusion in multi-layered aquifer as an advection-dispersion phenomenon, Proc. 8th International Symposium on Flow Modeling and Turbulence Measurements, pp.819-826, 2001.
14. Neuman, S. P.: Saturated unsaturated seepage by finite elements, Proc., ASCE HY, Vol.99, No.12, pp.2233-2250, 1973.
15. Neuman, S. P.: Galerkin method of analyzing non-steady flow in saturated-unsaturated porous media, Finite element Method in flow problem, edited by C. Taylor, O.C. Zienkiewicz, R.H. Gallagher, John Wiley & Sons, Chap.19, 1974.
16. Akai, K., Ohnishi, Y. and Nishigaki, M.: Finite Element Analysis of Saturated-Unsaturated Seepage in Soil, Proc. of JSCE, No.264, pp.87-96, 1977.
17. van Genuchten, M. T.: A closed-form equation for predicting the hydraulic conductivity of unsaturated soils, Soil Science Society of America Journal, Vol.44, pp.892-898, 1980.
18. Maulem, Y. :A new model for predicting the hydraulic conductivity of unsaturated porous media, Water Resour. Res., Vol.12, pp.513-522, 1976.
19. Bear, J. :Dynamics of Fluid in Porous Media, Elsevier, New York, 1972.
20. Zienkiewicz, O. C. and Taylor, R. L.: The Finite Element Method, Vol.3, (5th ed.), Butterworth-Heinemann, pp.13-63, 2000.
21. Saito, M. and Kawatani, T.: Theoretical Study on Spatial Distribution of Hydraulic Conductivity, Journal of Geotechnical Engineering, No.645/III-50, pp.103-114, 2000. (in Japanese)
22. Saito, M. and Kawatani, T.: Study on Applicability of Geostatistical Models of Hydraulic Conductivity, Journal of Geotechnical Engineering, No.694/III-57, pp.245-258, 2001. (in Japanese)
23. Saito, M. and Kawatani, T.: Simple method for generation of 1-D and 2-D random permeability field by using stochastic fractal model, Proc. of the 4th International conference on CALIBRATION AND RELIABILITY IN GROUNDWATER MODELING, Vol.1, pp.176-179, 2002.
24. Bear, J.: Hydraulics of Groundwater, McGraw-Hill, pp.379-435, 1979.

(Received Aug, 01, 2011 ; revised Mar, 12, 2012)